

# QUANTITATIVE MORPHOLOGY AT HIGH REDSHIFTS

Roberto G. Abraham

*Royal Greenwich Observatory, Madingley Road, Cambridge CB3 0EZ, UK*

**Abstract.** The current evidence for morphologically peculiar galaxy populations at high-redshifts is outlined. After describing various techniques which can be used to quantify the importance of “morphological K-corrections”, and to objectively classify galaxy morphology in the presence of these biases, it is concluded that observational biases are not sufficient to explain the increase in the fraction of peculiar galaxies on deep HST images. A new technique is then described which models the spatially resolved internal colors of high redshift galaxies, as a probe of the processes driving galaxy evolution. This “morphometric” approach investigates directly the evolutionary history of stellar populations, and is a sensitive test of the mechanisms through which galaxies build up and evolve in the field. As a case study, we analyse several “chain galaxies” in the Hubble Deep Field. These chain galaxies are shown to be protogalaxies undergoing their first significant episodes of star-formation, and not simply distant edge-on spirals.

## I INTRODUCTION

Recent work from deep imaging [15,14,10,2,3,13] and spectroscopic [17,7,18,11] surveys has shown that much of the rapidly evolving faint blue galaxy population [5,16,17] is comprised of morphologically peculiar galaxies. These systems may be luminous counterparts to local irregular galaxies, tidally disturbed systems, or perhaps members of entirely new classes of objects with no local counterpart. Another possibility is that these morphologically peculiar systems are simply “ordinary” galaxies whose strange appearance is simply a result of their being observed in the rest-frame ultraviolet (a “morphological K-correction”), where we know little about the appearance of the galaxy population. This distinction between intrinsic and apparent peculiar galaxies lies at the heart of this meeting. In this article several lines of evidence are reviewed which suggest that the bulk of the morphological peculiarities seen in distant galaxies are intrinsic to these systems, and not simply the product of rest-frame bandshifting. In the final section of this article preliminary results from a new line of evidence are presented, focussing on the “chain galaxy”

**FIGURE 1.** Comparison between the far-UV morphology “predicted” on the basis of *optical* colors of NGC1365 and the observed morphology from the Ultraviolet Imaging Telescope (UIT). Optical images were obtained from the 2.5m du Pont telescope on Las Campanas, and no noise has been added in order to match the signal-to-noise characteristics of the UIT.

population as a case study.

## II HIGH REDSHIFT GALAXY MORPHOLOGY

### A Quantitative Comparisons with Simulations

The first line of evidence is the result of a quantitative comparison between the observed morphologies of local galaxies and the predicted appearance of their *non-evolved* high-redshift counterparts. In order to undertake this comparison we have developed a technique for artificially redshifting local galaxy CCD images by assigning separate spectral energy distributions to individual pixels. Spectral energy distributions for each pixel are determined by using optical colors to interpolate between template spectra corresponding to local S0, Sab, Sbc, Scd, Sdm, and starbursting galaxies. Figure 1 illustrates the power of this technique by showing the excellent agreement between “predicted” and observed far-UV morphologies for a typical galaxy in our calibration sample<sup>1</sup>. This figure illustrates the extreme case in which the *I*-band morphology is extrapolated to the far-UV, corresponding to redshifts  $z > 4$ . In fact, at  $z > 4$  the galaxian internal dynamical timescale is a substantial fraction of the age of the Universe, so the existence of morphologically unevolved galaxies is not expected.

With this capability to model the effects of bandshifting on observed morphology, *and by assuming an approximate redshift distribution*, one is able account for the impact of morphological K-corrections on morphologically segregated deep number-magnitude counts. Because the subjective nature of visual classification makes comparisons between different groups susceptible to large systematic errors [20], the best approach to making these counts is to adopt a quantitative morphological classification system. Several quantitative classification systems have now been developed [1,3,21]. Figure 2 shows the number-magnitude counts which result from applying a particularly simple

---

<sup>1</sup>) In order to make a comparison with UIT straightforward, noise has not been added to the simulations. Because of  $(1+z)^4$  cosmological dimming extremely long exposure times with HST would be required to image this galaxy at high redshifts with a signal-to-noise level equivalent to that shown.

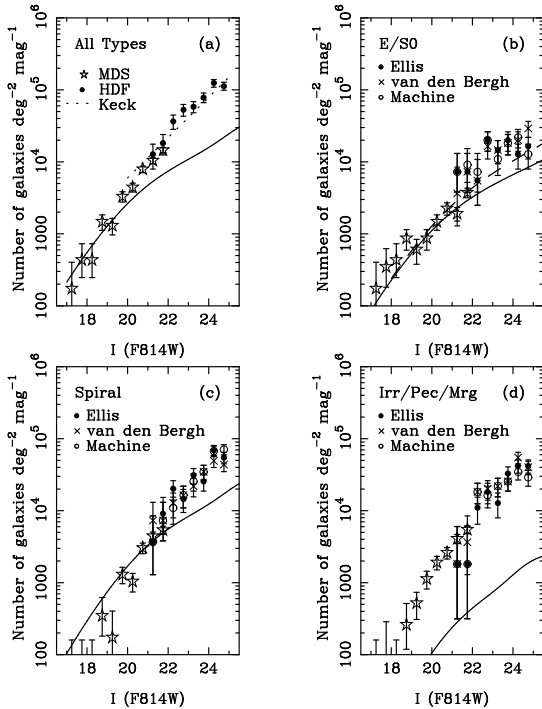


**FIGURE 2.** The number-magnitude relations for morphologically segregated samples of galaxies from the HDF and MDS (from Abraham *et al.* 1996a). Open circles indicate counts obtained from automated classifications, closed circles indicate the results from the visual classifications of Ellis, and crosses indicate the results from the visual classifications of van den Bergh. The MDS counts are indicated by the stars on each panel. The no-evolution  $\Omega = 1$  curves from Glazebrook *et al.* (1995), extrapolated to  $I = 25$  mag, are superposed. The dashed line on the E/S0 diagram shows the effect of assuming  $\Omega = 0.1$ . The dotted line in panel (a) shows the  $I$ -band number counts determined by Smail *et al.* (1995) from two deep fields imaged with the Keck telescope.

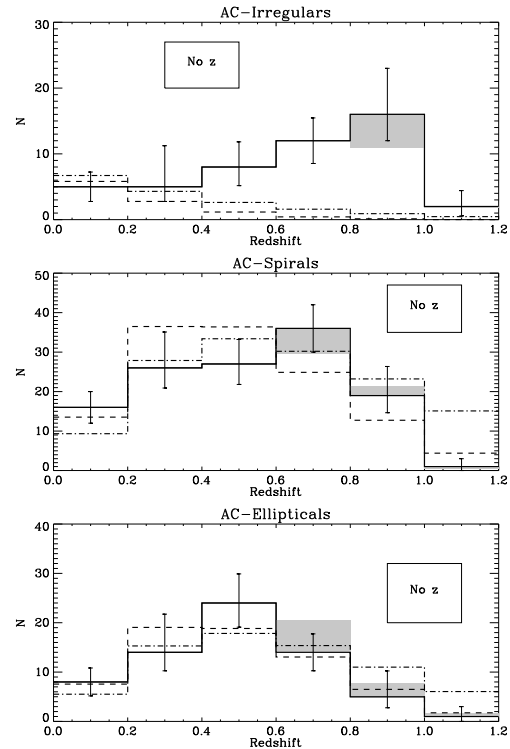


**FIGURE 3.** Morphologically segregated number counts from Brinchmann *et al.* 1997 (in preparation), based on data from the CFRS/LDSS collaboration. The bins show counts as a function of redshift for irregular/peculiar/merger systems (top), spirals (middle), and ellipticals (bottom). Morphological classifications have been made from WF/PC2 images using the central concentration vs. asymmetry system described in the text and in Abraham *et al.* 1996a. The shaded region corresponds to the size of the “morphological K-correction” on the classification. Superposed on the histograms are the predictions of no-evolution and 1 mag linear evolution to  $z = 1$  models.

system (based on measurements of central concentration,  $C$ , and asymmetry,  $A$ ) to data from the Hubble Deep Field. Also shown are the no-evolution predictions for ellipticals, spirals, and irregular/peculiar/merger systems, constructed as described in Glazebrook *et al.* (1995) and Abraham *et al.* (1996a,b), by adopting Schechter luminosity functions (LFs) with parameters given by Loveday *et al.* (1992), and a high normalization  $\phi_* = 0.03h^3 \text{ Mpc}^{-3}$ . The predicted counts for the elliptical galaxies are based on a flat slope ( $\alpha = -1$ ) for the faint-end of the LF, rather than the turn-over originally found by Loveday *et al.* The steep counts for the irregular/peculiar/merger systems continues to the limits of the survey. Beyond  $I_{814} = 22$  mag the spiral counts show a significant excess over the no-evolution predictions. A weaker trend is seen for the spheroidal systems (whose counts are only marginally above the no-evolution prediction) and there is some evidence of a turn-over in the last magnitude interval.

## B Redshift Surveys

The analysis presented in the previous section is fairly sensitive to the assumed redshift distribution of the peculiar galaxy population. However recent evidence from redshift surveys, most notably the Canada-France Redshift Survey (CFRS) suggests that, at least to  $I < 22$  mag (the typical morphologically resolved magnitude limit for deep HST imaging, prior to the Hubble Deep Field), the great majority of objects are at redshifts  $z < 1.5$  [18]. Therefore even quite deep HST WF/PC2  $I_{814}$ -band (the band most commonly used to quantify the morphological composition of the distant field) images should generally be compared with  $B$ -band or  $U$ -band local galaxy data. Since most local surveys of galaxy morphology are based on blue-sensitive photographic plates, the rest-frame  $B$ -band is in fact where we are most familiar with the appearance of galaxies, and the effects of bandshifting on these galaxies are likely to be less significant than the effects of limited signal-to-noise or binning. Images of local galaxies in  $U$ -band (blueward of the  $4000\text{\AA}$  break) are often substantially more irregular than  $B$ -band data, but they do not yet show the fantastic morphological variations (such as disappearing bulges) seen in images in the far-UV ( $\sim 1500\text{\AA}$ ), as presented by O'Connell and others at this conference.

This line of reasoning has recently been spectacularly confirmed [4] by Brinchmann *et al.* (1997), who have applied an objective classification scheme, again calibrated using pixel-by-pixel K-corrections, to a set of  $\sim 300$  HST  $I_{814}$ -band images of galaxies *with known redshifts* taken from the CFRS and LDSS [11] surveys. Because the statistical completeness of this sample is very well understood, reliable number-redshift histograms can be constructed for the various morphological types. The morphologically resolved  $n(z)$  result obtained by Brinchmann *et al.* is shown in Figure 3, and confirms that irreg-

ular/peculiar/merging systems are already greatly in excess of the predictions of no-evolution and mild-evolution models at redshifts  $z \sim 1$ . It is emphasized that: (a) because of the complete redshift information, morphological K-corrections have been accounted for explicitly for each galaxy in this study, and (b) in any case morphological K-correction effects cannot be dominant in this survey, because the peculiar excess is already large by  $z = 1$ , at which point one is only just beginning to probe into the ultraviolet.

### III MORPHOPHOTOMETRY

Studies of evolution in high-redshift galaxies have focused generally on either analyses of morphological characteristics, or on analyses of *integrated* colors using spectral synthesis techniques. While morphological studies often point the way forward, only rarely do they probe the underlying physics of galaxy evolution. On the other hand, studies of integrated colors are also limited, because galaxies are not homogeneous systems. Galaxy evolution can be described as a series of punctuated star-formation episodes whose imprints are recorded in distinct stellar populations (such as the disk and bulge), so studies which resolve these stellar populations are required in order to understand the mechanisms through which galaxies are built-up and evolve.

Therefore it seems that the important next step in understanding the history of galaxies is to unify morphological studies with stellar evolution modelling. In this section we present preliminary results from just such a *morphophotometric* analysis of the ‘‘chain galaxy’’ population. We have chosen to focus on this subset of the high-redshift peculiar galaxy population in this article because the controversy surrounding these systems is a perfect encapsulation of the theme of this meeting. In their discovery paper, Cowie and collaborators [7] claimed to have found a significant new young population of galaxies at high redshifts. This claim was immediately disputed [9]. Dalcanton & Shectman (1996) claim that chain galaxies are simply the distant counterparts to local edge-on low surface-brightness spiral galaxies. Can the internal colors of these systems shed light on the nature of these objects?

#### A Resolved Color Modelling

Consider the central equation of population synthesis [6], commonly used to model spectral evolution in galaxies:

$$F_\lambda(T) = \int_0^T \Psi(T - \tau) f_\lambda(\tau) d\tau. \quad (1)$$

In this formulation the emergent flux from a galaxy,  $F_\lambda$ , at time  $T$  is described by the convolution of the spectrum of an evolving instantaneous

starburst,  $f_\lambda(t)$ , with an assumed star-formation rate (SFR) function  $\Psi(t)$ . The  $f_\lambda(t)$  term is in principle known for various choices of initial mass function (IMF) and metallicity, using libraries of template stellar spectra and isochrones. Hierarchical formation scenarios suggest that stellar populations become built up over time, so in reality the age  $T$  of a galaxy is not a constant, and the distribution of internal colors is a partial record of the formation timescale(s) of the system. This age information for a given stellar population is diluted by the convolution with  $\Psi(t)$ , whose form is usually unknown. But in regions where the resolution is high enough to resolve the sites of current star-formation, or where mixing of multiple generations of stars has not occurred,  $\Psi(t)$  can be approximated by a  $\delta$ -function, breaking the convolution degeneracy in Equation 1, and allowing direct measurement the age distribution and form of  $f_\lambda(t)$ . Consider, for example, the canonical picture of a late-type spiral galaxy, where the bulk  $\Psi(t)$  can be well-approximated by a constant star-formation rate. This “constant” overall star formation rate is physically simply a time-average over the appearance and disappearance of spatially distinct HII regions and star-formation complexes, each of which individually can be considered to be a bursting simple stellar population with a lifetime (before disruption or gas depletion) that is short compared to the dynamical timescale of the galaxy. Therefore the distribution of colors for individual resolved young stellar associations on a color-color diagram directly maps out the shape of  $f_\lambda(t)$  for a set of young ages, giving direct access to the integrand of Equation 1 without first filtering by a convolution. As these stellar associations age and disappear the convolution with  $\Psi(t)$  in Equation 1 becomes important, as young stars become assimilated into older galactic components (ie. the disk and bulge) and are spatially averaged with earlier generations of stars. The distribution of colors for older stellar populations ( $\gtrsim 1$  Gyr) are therefore expected to trace out a continuous age track on the color-color diagram. The *shape* of this track for older stellar populations is in effect a measurement of the form of the star-formation law  $\Psi(t)$ , while the *distribution* of colors along this track is a record of the uniformity with which episodes of star formation have added to the stellar population (*e.g.* via numerous small bursts, or a smaller number of larger bursts).

Figure 4 shows the resolved color-color diagram for two rather typical spiral and elliptical galaxies in the HDF. These exhibit star-formation characteristics that are in reasonable agreement with our expectations based on studies of stellar populations in local galaxies. For example, the spiral galaxy is well described by a roughly constant star formation history. The bulge is the oldest component of this system, has a small dispersion in color, and is several Gyr older than the disk. By contrast the elliptical system shown is well described by an exponential star-formation history with a short e-folding timescale (around  $\tau = 1$  Gyr.) This system is apparently rather old and (from the small dispersion in color), all parts of the galaxy are well mixed and roughly coeval. The majority of spirals and ellipticals in the Hubble Deep Field exhibit

## Canonical Spiral and Elliptical Galaxies

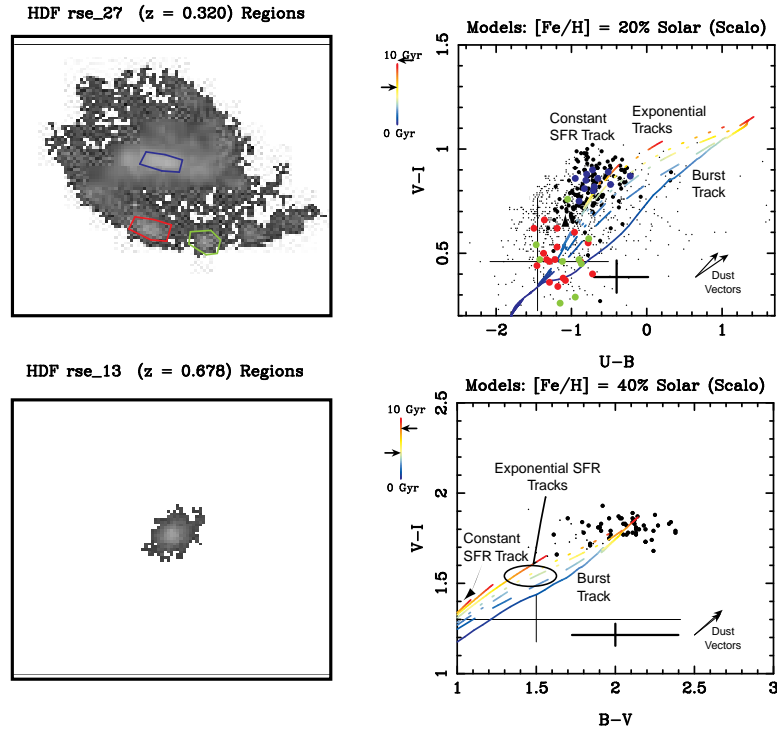


**FIGURE 4.** Morphometric color-color diagrams for two “canonical” galaxies in the Hubble Deep Field. The panels on the left show  $I$ -band images of the galaxies, “segmented” from the background sky by isophotal thresholding. The right hand panels show the color-color diagrams for *individual pixels* in the galaxy. The data points have been subdivided into high signal-to-noise (SNR) pixels [circles] and low signal-to-noise pixels [dots]. The mean error bars for the high SNR and low SNR points are shown by the dark and light error bars. Model tracks are also shown on the right, and are calibrated to age in Gyr [keyed to the color bar]. Arrows on the color bar indicate the age of the Universe in the rest frame of the galaxy, for  $H_o = 70$  km/s/Mpc and  $\Omega = 0.1$  and  $\Omega = 1$ . The dust vectors (for LMC and SMC extinction laws) shown correspond to an extinction of  $A_B = 0.2$  mag in the rest frame of the galaxy. The colored points shown on the color-color diagram for the spiral galaxy correspond to pixels inside the colored polygons shown on the left hand panel.

morphophotometric diagrams qualitatively similar to those shown in Figure 4.

## B The Nature of Chain Galaxies

Figure 5 shows a montage of resolved color-color diagrams for the three “chain galaxies” (as visually classified by R. Ellis) with known redshifts in the Hubble Deep Field<sup>2</sup>. The morphophotometric analysis shown in this figure indicates that these systems are likely to be very young galaxies recovering from their first star-formation episodes. Unlike the case for late-type galaxies exhibiting knots of star-formation superposed on a disk (as shown in Figure 4), there is no evidence for an underlying “old” component in any of these systems. Using the surface brightness detection threshold for the  $I_{814}$  data, we can place an upper limit of  $< 10\%$  for the contribution of old stars to the total baryonic mass of two systems at  $z < 1.5$  systems shown in this figure<sup>3</sup>. All components of the chain galaxies lie close to the “pure” starburst track: evidently rather little mixing of young components within the body of the galaxy as occurred. (This mixing would show up as a dispersion along the exponential or constant star formation tracks, as populations with different ages blend together). Intriguingly, the knots of star-formation in the lower-redshift chains appear to be synchronized, both spatially and temporally. Star-formation has been triggered along the body of these system like a string of fireworks. The oldest knots in the  $z < 1.5$  systems appear to have ignited the other knots in sequence along the body of the galaxies. In all cases shown the unweighted mean age of the starlight in the galaxy is 100-200 Myr (comparable with the dynamical timescale of the galaxy), with the youngest and oldest knots in the chain differing in age by around 30-50 Myr. *This morphophotometric analysis indicates that these chain galaxies are likely to be stochastically ignited very young galaxies, and not edge-on low-surface brightness spirals, as has been claimed.* Although it is important to bear in mind that the three systems presented in this article may not be representative of the class (being taken from an incomplete redshift survey, with strong biases toward strong emission-line systems), it appears that at least *some* chain galaxies (*i.e.* all chain galaxies in the redshift sample to date) are protogalactic starburst systems.

---

<sup>2</sup>) HDF redshifts discussed in this article were taken from the 55 redshifts available on the World Wide Web as of April 1997.

<sup>3</sup>) Strong upper limits cannot be placed on a putative old component underlying the “hot dog” Lyman limit system at  $z = 2.803$  shown in Fig. 5, because of strong K-corrections for red light at  $z > 2$ . However, depending on  $\Omega$ , restrictions on such a component may be imposed by the age of the Universe in the rest frame.



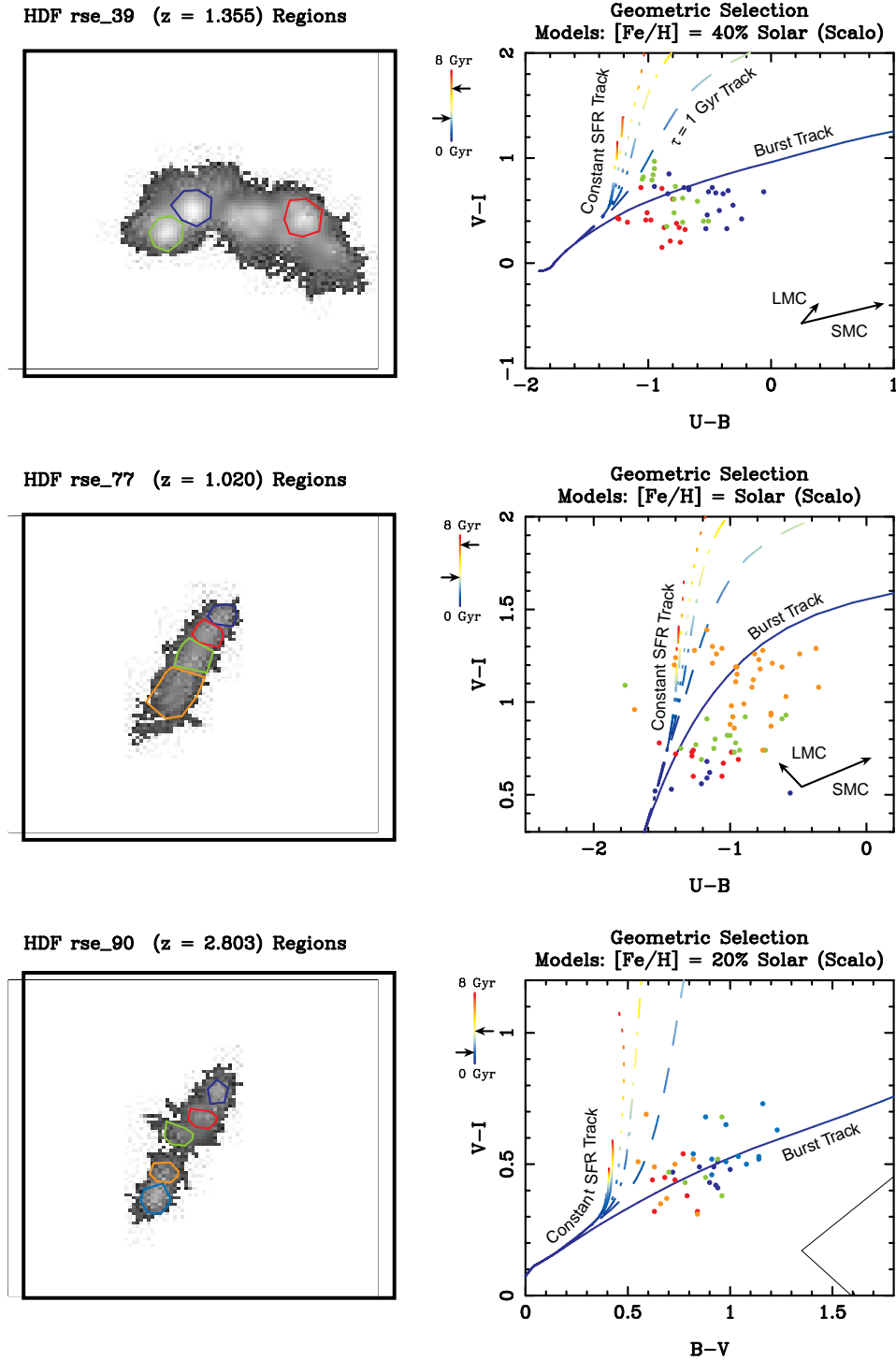


**FIGURE 5.** Morphophotometric color-color diagrams for the three “chain galaxies” in the public database of HDF redshifts. The right-hand panels show the distribution of pixel colors within the regions of the galaxy defined on the left-hand panels. Also shown on the right are models corresponding to constant star formation, exponential star formation, and an instantaneous starburst. See also the caption for the previous figure.

## CONCLUSIONS

The taxonomy of peculiar galaxies is confusing and possibly inconsistent, but studies using objective classifications calibrated by simulations offer a way forward. These studies show that contamination by bandshifted late-type galaxies into samples of “peculiar” galaxies is small until  $z \sim 1.5$ , at which point the observed fraction of irregular/peculiar/merging systems is already much higher than predicted on the basis of no-evolution models. We therefore conclude that “morphological K-corrections” are a second-order effect, and do not account for the proportion of irregular/peculiar/merging systems seen on deep HST images. At higher redshifts contamination by bandshifted spirals may be more important, although genuinely protogalactic systems are definitely seen. At least some “chain galaxies” are protogalaxies – strongly starbursting systems forming their first generation of stars – and *not* not edge-on low surface brightness systems.

**Acknowledgments** I thank my collaborators Richard Ellis, Jarle Brinchmann, Karl Glazebrook, Andy Fabian, Sidney van den Bergh, Nial Tanvir, and Basilio Santiago for their many contributions to the projects described in this article. I am also grateful to Simon Lilly and the rest of the CFRS team for useful discussions, and for permission to describe results in advance of publication.

## REFERENCES

1. Abraham, R.G., Valdes, F., Yee, H.K.C. & van den Bergh, S. 1994, ApJ, 432, 75
2. Abraham, R. G, Tanvir, N. R., Santiago, B. X. , Ellis, R. S., Glazebrook, K. & van den Bergh, S. 1996a, MNRAS, 279, L47
3. Abraham, R.G., van den Bergh, S., Glazebrook, K., Ellis, R.S., Santiago, B. X., Surma, P., & Griffiths, R. 1996b, ApJSupp, 107, 1.
4. Brinchmann, J. *et al.* 1997. In preparation.
5. Broadhurst, T., Ellis, R., & Shanks, T. 1988, MNRAS, 235, 827
6. Bruzual, G., & Charlot, S. 1993, ApJ, 378, 471
7. Cowie, L. L., Hu, E. M., & Songaila, A. 1995, AJ, 110, 1576.
8. Cowie, L. L., Songaila, A., Hu, E. M., & Cohen, J. D. 1996, AJ, 112, 834
9. Dalcanton, J. J., & Shectman, S. A. 1996, ApJ, 465, 9
10. Driver, S.P., Windhorst, R.A. & Griffiths, R.E. 1995, ApJ, 453, 48.
11. Ellis, R. S., Colless, M., Broadhurst, T., Heyl, J., & Glazebrook, K. 1996, MNRAS, 280, 235
12. Frei, Z., Guhathakurta, P., Gunn, J. E. 1996, AJ, 111, 174
13. Giavalisco, M., Steidel, C. C., & Macchetto, F. D. 1996, ApJ, 470, 189
14. Glazebrook, K., Ellis, R., Santiago, B. & Griffiths, R. 1995, MNRAS, 175, L19.
15. Griffiths, R.F. *et al.* 1994, ApJ, 437, 67.

16. Koo, D. C., & Kron, R. 1992, *Ann. Rev.* 30, 613.
17. Lilly, S. J., Tresse, L., Hammer, F., Crampton, D., Le Fèvre, O. 1995, *ApJ*, 455, 108
18. Lilly, S. J., Le Fèvre, O., Hammer, F., & Crampton, D. 1996, *ApJ*, 460, L1
19. Loveday, J., Peterson, B. A., Efstathiou, G., Maddox, S. J. 1992, *ApJ*, 390, 338
20. Naim, A., *et al.* 1995 , *MNRAS*, 274, 1107
21. Odewahn, S. C., Windhorst, R. A., Driver, S. P., & Keel, W. C. 1996. *Nature*, 383, 45.

This figure "n1365\_uv\_b\_i\_model.jpg" is available in "jpg" format from:

<http://arxiv.org/ps/astro-ph/9802036v1>